JOURNAL OF COMPUTATIONAL PHYSICS 87, 464–487 (1990)

Dynamics of Shear Flow of a Non-Newtonian Fluid*

DAVID S. MALKUS,† JOHN A. NOHEL,‡ AND BRADLEY J. PLOHR§

Center for the Mathematical Sciences, University of Wisconsin-Madison, Madison, Wisconsin 53705

Received October 11, 1988; revised February 27, 1989

DEDICATED TO R. BYRON BIRD ON HIS 65TH BIRTHDAY

Viscoelastic materials with fading memory, e.g., polymers, suspensions, and emulsions, exhibit behavior that is intermediate between the nonlinear hyperbolic response of purely elastic materials and the strongly diffusive, parabolic response of viscous fluids. Many popular numerical methods used in the computation of steady viscoelastic flows fail in important flow regimes, and thus do not capture significant non-Newtonian phenomena. A key to satisfactory explanation of these phenomena is the study of the full dynamics of the flow. This paper studies the dynamics of shear flow, presenting a description of non-Newtonian phenomena caused by a non-monotone relation between the steady shear stress and shear strain rate. Analytical results for such phenomena are surveyed, and three distinct numerical methods are developed to accurately compute the dynamics. The computations reproduce experimental measurements of non-Newtonian "spurt" in shearing flow through a slit die. They also predict related phenomena (such as hysteresis and shape memory); experiments are suggested to verify these predictions.

1. INTRODUCTION

Viscoelastic materials with fading memory, e.g., polymers, suspensions, and emulsions, exhibit behavior that is intermediate between the nonlinear hyperbolic response of purely elastic materials and the strongly diffusive, parabolic response of viscous fluids. Their properties reflect a subtle dissipative mechanism induced by the fading memory. Several interesting physical phenomena, which are important, for example, in polymer processing, arise in shear flows of viscoelastic fluids. Understanding such phenomena has proved to be of significant physical, mathematical, and computational interest. We have found that satisfactory explanation and

* Supported by the U.S. Army Research Office under Grant DAAL 03-87-K-0036, the National Science Foundation under Grants DMS-8712058 and DMS-8620303, and the Air Force Office of Scientific Research under Grants AFOSR-87-0191 and AFOSR-85-0141.

† Also Department of Engineering Mechanics.

‡ Also Department of Mathematics.

§ Also Computer Sciences Department.

0021-9991/90 $3.00

modeling requires the study of the full dynamics of the equations of motion and the constitutive assumptions.

One striking phenomenon has been observed by Vinogradov *et al.* [20] in the flow of viscoelastic fluids (monodisperse polyisoprenes) through capillaries. They found that the volumetric flow rate increased dramatically at a critical stress that was independent of molecular weight. This phenomenon, which is called "spurt," had been overlooked or dismissed by rheologists because no plausible mechanism was known to explain it in the context of steady flows. Spurt was lumped together with instabilities such as "slip," "apparent slip," and "melt fracture," which are poorly understood. While regarded as anomalous, these instabilities can severely disrupt polymer processes; they can be avoided in practice only with ad hoc engineering expedients. The mechanisms of such phenomena are not understood; this is because the governing equations are analytically intractable and because many numerical methods for steady viscoelastic fluid flows falter in this regime and thus cannot model the spurt phenomenon.

Several explanations have been offered for the spurt phenomenon [2, 4, 10, 13]. Their common feature is that the shear stress in steady flow does not vary monotonically with shear strain rate (as illustrated in Fig. 2, below). These explanations have been rejected be many rheologists as being somehow unphysical. We believe that this criticism is unfounded because it is based on intuition derived from generalized Newtonian models of non-Newtonian fluids. Our view is shared by Pearson [16], who discussed how non-monotone constitutive relations might explain various processing instabilities, including spurt. Pearson pointed out that non-monotone relations need not violate the laws of thermodynamics; he constructed a model with a gap of inaccessible shear rates and speculated that it exhibits flow instabilities. Our work shows that a relatively simple model, which submits to a complete analysis, produces these effects.

A key to understanding the spurt phenomenon is the dynamical behavior of the constitutive relations as well as the equations of motion. While there is a great variety of constitutive models for viscoelastic fluids, the dynamical behavior for many is difficult to analyze or compute. In this paper, we model the spurt phenomenon using the Johnson–Segalman model [8] of a non-Newtonian fluid. This constitutive relation correctly models the spurt phenomenon and yet is sufficiently simple to be understood through a combination of analysis, asymptotics, and numerical simulation. A non-monotone stress–strain-rate relation of the kind that causes the spurt phenomenon arises when the fluid behavior is characterized by multiple relaxation times. Interpretation of small-amplitude oscillatory shear data in Ref. [20] indicates that the relaxation times are widely spaced. Formal asymptotic analysis [11] of the dynamics shows that the effects of the smallest relaxation time are mimicked by a Newtonian viscosity term. For simplicity, then, we study the Johnson–Segalman model with a single relaxation time and added Newtonian viscosity.

We study idealized shearing flow through a narrow slit die. Assuming that the driving pressure is transmitted instantaneously, the three-dimensional flow may be

approximated by a one-dimensional problem. Our analytical and numerical results show that flow in a slit die reflects the essential features observed for capillaries. We believe that this is because the spurt phenomenon depends solely on material properties and the smallest physical dimension of the problem.

The outline of this paper is as follows. In Section 2, we describe the modeling of shearing flow of a viscoelastic fluid using the Johnson–Segalman constitutive relation. Mathematical results for this model, as well as for related models that capture some key features, are surveyed in Section 3. These include evolutionarity of the system, existence and regularity of solutions, formation of discontinuities, asymptotic behavior for large time, stability of steady solutions, structure of discontinuous solutions, and dynamics of a related system of ordinary differential equations. In Section 4, we develop three distinct numerical methods for solving the flow equations, accounting for the mathematical structure of the model. That these methods reproduce physical phenomena is demonstrated in Section 5, where we compare numerical calculations with experimental data for the spurt phenomenon. Based on these results, we propose in Section 6 some rheological experiments to confirm the predictions of the model. Finally, in Section 7, we discuss our conclusions.

2. Mathematical Formulation

2a. *Shear Flow of a Johnson–Segalman Fluid*

The motion of a fluid under incompressible and isothermal conditions is governed by the balance of linear momentum

$$\rho\left[\frac{\partial \mathbf{v}}{\partial t}+\mathbf{v}\cdot\nabla\mathbf{v}\right]=\nabla\cdot\mathbf{S}. \tag{2.1}$$

Here, ρ is the fluid density, $\mathbf{v}$ is the particle velocity, and $\mathbf{S}$ is the stress tensor. The response characteristics of the fluid are embodied in the constitutive relation for the stress. For viscoelastic fluids with fading memory, these relations specify the stress as a functional of the deformation history of the fluid. Many sophisticated constitutive models have been devised; see Ref. [1] for a survey. In the present work, we focus on the Johnson–Segalman model [8] as a prototype for general constitutive models. This model accounts for non-affine deformation of Gaussian networks by introducing a slip parameter a, $-1\leqslant a\leqslant 1$, leading to a nonlinear generalization of the classical Maxwell model.

To specify this constitutive relation, we decompose the stress as

$$\mathbf{S}=-p\mathbf{I}+2\eta\mathbf{D}+\boldsymbol{\Sigma}. \tag{2.2}$$

In this equation, p is an isotropic pressure (which is determined from the incompressibility constraint), η is the coefficient of Newtonian viscosity, and $\boldsymbol{\Sigma}$ is the non-

Newtonian extra stress. Also, we let $\mathbf{D} := \frac{1}{2}[\nabla\mathbf{v} + (\nabla\mathbf{v})^{\mathrm{T}}]$ and $\mathbf{\Omega} := \frac{1}{2}[\nabla\mathbf{v} - (\nabla\mathbf{v})^{\mathrm{T}}]$ be the symmetric and antisymmetric parts of the velocity gradient $\nabla\mathbf{v}$, which has components $(\nabla\mathbf{v})^i_j := \partial v^i/\partial x^j$. The extra stress is specified by the differential constitutive law

$$\overset{*}{\mathbf{\Sigma}} = 2\mu\mathbf{D} - \lambda\mathbf{\Sigma}, \tag{2.3}$$

where

$$\overset{*}{\mathbf{\Sigma}} := \frac{\partial\mathbf{\Sigma}}{\partial t} + \mathbf{v}\cdot\nabla\mathbf{\Sigma} + \mathbf{\Sigma}[\mathbf{\Omega} - a\mathbf{D}] + [\mathbf{\Omega} - a\mathbf{D}]^{\mathrm{T}}\,\mathbf{\Sigma} \tag{2.4}$$

is the objective time derivative of $\mathbf{\Sigma}$ with parameter a. The parameter μ is an elastic shear modulus, and λ is a relaxation rate.

Constitutive relations such as Eq. (2.3) exhibit a mixture of elastic and viscous behavior. This may be seen heuristically as follows. In the long relaxation-time limit, $\lambda \to 0$, Eq. (2.3) shows that an objective time derivative of $\mathbf{\Sigma}$ is proportional to the deformation rate: $\overset{*}{\mathbf{\Sigma}} \sim 2\mu\mathbf{D}$. This is characteristic of elastic behavior, and leads to the interpretation of μ as a shear modulus. By contrast, when $\lambda,\ \mu \to \infty$ with μ/λ fixed, $\mathbf{\Sigma} \sim 2(\mu/\lambda)\,\mathbf{D}$; thus the model displays viscous behavior with μ/λ being the Newtonian shear viscosity coefficient.

Essential properties of the constitutive relation are exhibited in simple planar shear flow. With the flow aligned along the y-axis (see Fig. 1), the flow variables are independent of y. Therefore the velocity field is $\mathbf{v} = (0, v(x, t))$, and the balance of mass is automatically satisfied. Furthermore, the components of the extra stress tensor $\mathbf{\Sigma}$ may be written $\Sigma^{xx} = \gamma(x, t)$, $\Sigma^{xy} = \Sigma^{yx} = \sigma(x, t)$, and $\Sigma^{yy} = \tau(x, t)$, while the pressure takes the form $p = p_0(x, t) - f(t)\,y$, f being the pressure gradient driving the flow. In these terms, Eqs. (2.3) become

$$\gamma_t + (1-a)\,\sigma v_x = -\lambda\gamma, \tag{2.5a}$$

$$\sigma_t - [\tfrac{1}{2}(1+a)\,\gamma - \tfrac{1}{2}(1-a)\,\tau + \mu]\,v_x = -\lambda\sigma, \tag{2.5b}$$

$$\tau_t - (1+a)\,\sigma v_x = -\lambda\tau. \tag{2.5c}$$

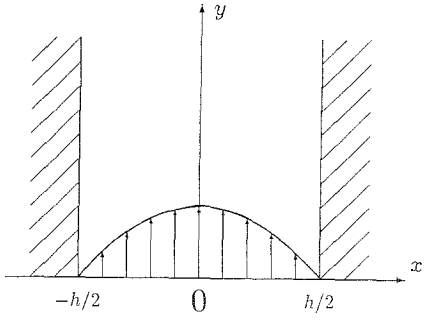

FIG. 1. Shear flow through a slit-die.

Introducing the variables $Z := \frac{1}{2}(1+a)\gamma - \frac{1}{2}(1-a)\tau$ and $W := -\frac{1}{2}(1+a)\gamma - \frac{1}{2}(1-a)\tau$, Eqs. (2.5) simplify to

$$\sigma_t - (Z+\mu)\, v_x = -\lambda\sigma, \tag{2.6a}$$

$$Z_t + (1-a^2)\,\sigma v_x = -\lambda Z, \tag{2.6b}$$

$$W_t = -\lambda W. \tag{2.6c}$$

Because W must remain finite as $t \to -\infty$, $W \equiv 0$, and the last equation may be omitted. As a result, $Z = -\frac{1}{2}(1-a^2)(\tau - \gamma)$, where $\Sigma^{yy} - \Sigma^{xx} = \tau - \gamma$ is the principal normal stress difference.

Combining the constitutive law (2.6) with the balance of linear momentum (2.1), we are led to the system of equations

$$\rho v_t - \sigma_x = \eta v_{xx} + f, \tag{2.7a}$$

$$\sigma_t - (Z+\mu)\, v_x = -\lambda\sigma, \tag{2.7b}$$

$$Z_t + (1-a^2)\,\sigma v_x = -\lambda Z. \tag{2.7c}$$

In this paper, we study shear flow between two parallel plates, located at $x = \pm h/2$. By symmetry, we need only consider the flow on the interval $[-h/2, 0]$. The no-slip condition at the plate implies the boundary condition $v(-h/2, t) = 0$, while symmetry imposes that $v_x(0, t) = 0$. We also prescribe initial values for v, σ, and Z, which must be compatible with the boundary conditions. To conform with the symmetry, we require that $\sigma(0, 0) = 0$; then, according to Eq. (2.7b), $\sigma(0, t) = 0$ for all time.

To eliminate unnecessary parameters, we scale distance by h, time by λ^{-1}, and the stresses σ and Z by μ. Furthermore, if we replace σ, v, and f by $\hat{\sigma} := (1-a^2)^{1/2}\,\sigma$, $\hat{v} := (1-a^2)^{1/2}\, v$, and $\hat{f} := (1-a^2)^{1/2} f$, respectively, then the parameter a disappears from Eqs. (2.7). Since no confusion will arise, we omit the caret. The dimensionless parameters are $\alpha := \rho h^2 \lambda^2/\mu$ and $\varepsilon := \eta\lambda/\mu$. Consequently, we study the initial-boundary-value problem for the system

$$\begin{aligned} \alpha v_t - \sigma_x &= \varepsilon v_{xx} + f, \\ \sigma_t - (Z+1)\, v_x &= -\sigma, \\ Z_t + \sigma v_x &= -Z, \end{aligned} \tag{JS}$$

on the interval $[-1/2, 0]$, with boundary conditions

$$v(-1/2, t) = 0 \qquad \text{and} \qquad v_x(0, t) = 0 \tag{BC}$$

and initial conditions

$$v(x, 0) = v_0(x), \qquad \sigma(x, 0) = \sigma_0(x), \qquad Z(x, 0) = Z_0(x), \tag{IC}$$

where $v_0(-1/2)=0$, $v_0'(0)=0$, and $\sigma_0(0)=0$. For later purposes, notice that the momentum equation may be written $\alpha v_t - T_x = f$, where $T := \sigma + \varepsilon v_x$ denotes the total shear stress.

2b. *Steady Shear Flow*

The steady-state solutions of (JS), when the forcing term f is a constant $\bar{f}$, play an important role in our discussion. Such a solution, denoted by $\bar{v}$, $\bar{\sigma}$, and $\bar{Z}$, is given as follows. The stress components $\bar{\sigma}$ and $\bar{Z}$ are related to the velocity gradient $\bar{v}_x$ (which, in dimensionless units, is the Deborah number) through

$$\bar{\sigma} = \frac{\bar{v}_x}{1+\bar{v}_x^2} \tag{2.8}$$

and

$$\bar{Z} + 1 = \frac{1}{1+\bar{v}_x^2}. \tag{2.9}$$

Therefore the total steady shear stress $\bar{T} := \bar{\sigma} + \varepsilon \bar{v}_x$ is given by $\bar{T} = T_{\text{steady}}(\bar{v}_x)$, where

$$T_{\text{steady}}(\bar{v}_x) := \frac{\bar{v}_x}{1+\bar{v}_x^2} + \varepsilon \bar{v}_x. \tag{2.10}$$

When $\varepsilon < 1/8$, this relation between the steady shear stress and strain rate is not monotone, as illustrated in Fig. 2. In this manner, the "stress loop" of Fig. 2 arises automatically in the Johnson–Segalman model.

The momentum equation, together with the boundary condition at the centerline, implies that the total steady shear stress satisfies $\bar{T} = -\bar{f}x$ for $x \in [-\frac{1}{2}, 0]$. Therefore the velocity gradient may be determined as a function of x by solving

$$T_{\text{steady}}(\bar{v}_x) = -\bar{f}x. \tag{2.11}$$

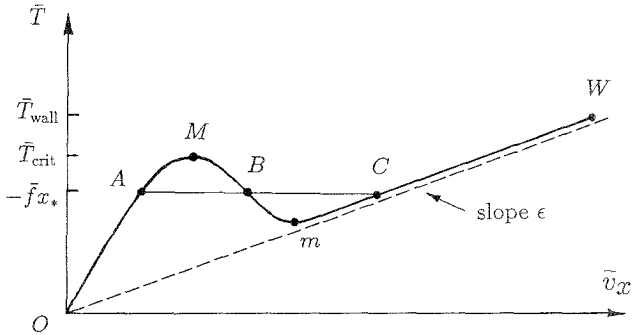

FIG. 2. Total steady shear stress $\bar{T}$ vs. shear strain rate $\bar{v}_x$ for steady flow.

The steady velocity profile, shown in Fig. 3, is obtained by integrating $\bar{v}_x$ and using the boundary condition at the wall. However, because the function T_{steady} is not monotone, there may be up to three distinct values of $\bar{v}_x$ that satisfy Eq. (2.11) for any given x. Consequently, $\bar{v}_x$ may suffer jump discontinuities, resulting in kinks in the velocity profile (as at the point x_* in Fig. 3). Indeed, a steady solution must contain such a jump if the total stress $\bar{T}_{\text{wall}} = \bar{f}/2$ at the wall exceeds the total stress at the local maximum in Fig. 2; for later convenience, we denote this critical stress by $\bar{T}_{\text{crit}} = \bar{f}_{\text{crit}}/2$.

2c. *Comparison with the Generalized Newtonian Model*

Traditionally, a non-monotone relation between stress and strain rate is regarded as a defect of the constitutive law. This conclusion is based on intuition appropriate for generalized Newtonian models of non-Newtonian fluids. Shear flow for such a fluid is governed by the single equation

$$\rho v_t - [\eta(v_x)\, v_x]_x = f, \tag{2.12}$$

corresponding to having a viscosity coefficient η that depends on strain rate. In a flow regime where $\eta(v_x)\, v_x$ decreases with strain rate v_x, however, Eq. (2.12) has the character of a backward heat equation, which suffers from the Hadamard instability. Therefore for generalized Newtonian fluids, $\eta(v_x)\, v_x$ must increase with v_x in a physically stable steady solution.

The system (JS) has the same steady solutions as a generalized Newtonian model with $\eta(v_x)\, v_x = T_{\text{steady}}(v_x)$, so one might think that it exhibits the same instability in regions where T_{steady} decreases. This conclusion is not warranted, however, because the system (JS) maintains its evolutionary character when $\varepsilon > 0$ (see Section 3a).

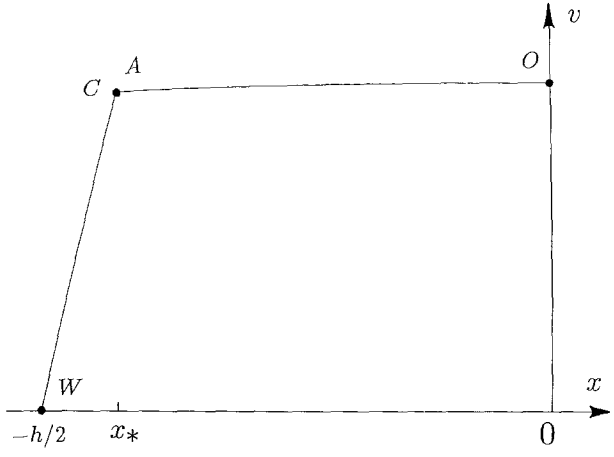

FIG. 3. Velocity profile for steady flow.

3. Mathematical Results

Several mathematical results are known for the system (JS); we refer to Refs. [6, 19, 4, 18, 3, 15, 11] for further discussions and additional references.

3a. *Evolutionarity, Existence of Solutions, and Formation of Discontinuities*

When the viscosity parameter $\varepsilon = 0$, the quasi-linear system (JS) is strictly hyperbolic provided that $Z + 1 > 0$. In this case, the wave speeds are $\pm [(Z+1)/\alpha]^{1/2}$ and zero. If, on the other hand, $Z+1$ becomes negative, then (JS), with $\varepsilon = 0$, undergoes a change of type and loses its evolutionary character. Joseph, Renardy, and Saut [6] have associated this change of type with certain fluid instabilities. Notice, however, that $Z + 1 > 0$ for steady flows, according to Eq. (2.9). A similar result holds for two-dimensional flows: Joseph and Saut [7] have demonstrated that flows perturbing plane Poiseuille flow of a Johnson–Segalman fluid do not lose evolutionarity.

Suppose that $\varepsilon = 0$ and $f = 0$, and assume that the initial data are smooth and lie in the hyperbolic region. If the data have sufficiently small variation, then a unique classical solution of (JS), (IC), (BC) exists globally in time; moreover, the solution decays to zero as $t \to \infty$. This can be proved using the energy methods discussed in Ref. [19]. On the other hand, if the data have sufficiently large variation, then the classical solution blows up within finite time; i.e., $|v_x|$, $|\sigma_x|$, and $|Z_x|$ approach infinity as t approaches a finite critical time. This is proved in Ref. [19] using the method of characteristics. Thus the fading memory acts as a weak dissipative mechanism: the source terms in the equations serve to counteract the formation of singularities from sufficiently smooth data. When discontinuities do form, system (JS) is no longer valid because the products of distributions Zv_x and σv_x are ill-defined. (See the discussion in Section 3b.)

If $\varepsilon > 0$, the system (JS) is evolutionary, but it cannot be classified according to type. Recently, Guillopé and Saut [3] established the global existence of solutions of (JS) for planar Couette and Poiseuille flow with data of arbitrary size. They also studied the asymptotic (Lyapunov) stability of steady states in the Couette case.

3b. *Conservation Laws*

It is important to observe that (JS) is not in conservation form. The evolution of a Johnson–Segalman fluid is, in fact, governed by physical conservation laws [8]. A conservative formulation of (JS) must be used when σ, v, and Z are discontinuous.

Following Plohr [18], we introduce the "elastic part" τ of the shear strain and the "entropy" variable z through the relations

$$\sigma := z \sin \tau, \tag{3.1a}$$

$$Z + 1 := z \cos \tau. \tag{3.1b}$$

Then system (JS) is transformed into the equivalent system

$$\begin{aligned} \tau_t - v_x &= -z^{-1}\sin\tau, \\ \alpha v_t - [\sigma(\tau, z) + \varepsilon v_x]_x &= f, \\ z_t &= -(z - \cos\tau), \end{aligned} \tag{C}$$

which is in conservative (i.e., divergence) form. Furthermore, if the internal energy $\mathscr{E}$ is defined by

$$\alpha\mathscr{E} := 1 - z\cos\tau, \tag{3.2}$$

the energy is dissipated according to the equation

$$\alpha[\tfrac{1}{2}v^2 + \mathscr{E}(\tau, z)]_t - \{[\sigma(\tau, z) + \varepsilon v_x]\, v\}_x = vf - \alpha\mathscr{E}(\tau, z) - \varepsilon(v_x)^2. \tag{3.3}$$

The conservative formulation (C) of (JS) is used in the numerical methods discussed in Section 4c.

3c. *Model Problems*

More detailed analytical results are obtained by simplifying the system (JS). A model system that incorporates several qualitative features of (JS) is obtained by freezing Z at its equilibrium value: $Z + 1 = 1/(1 + v_x^2)$. Defining $g(v_x) := v_x/(1 + v_x^2)$, system (JS) becomes

$$\begin{aligned} \alpha v_t - \sigma_x &= \varepsilon v_{xx} + f, \\ \sigma_t - g(v_x) &= -\sigma. \end{aligned} \tag{M}$$

More generally, g may be any smooth, odd function. The boundary and initial conditions for v and σ are the same as in (BC) and (IC). We assume that $\varepsilon > 0$ and that f is the constant $\bar{f}$. The function g is related to the steady stress–strain-rate relation through $T_{\text{steady}}(\bar{v}_x) = g(\bar{v}_x) + \varepsilon\bar{v}_x$. A steady solution of (M) satisfies $\bar{\sigma} = g(\bar{v}_x)$ and $T_{\text{steady}}(\bar{v}_x) = -\bar{f}x$, just as for the system (JS).

Nohel, Pego, and Tzavaras [15] have shown that the global classical solution v, σ of (M), (BC), (IC) has the following properties:

(i) With $S := \sigma + \varepsilon v_x + \bar{f}x$, $S(x, t) \to 0$ as $t \to \infty$, uniformly for $x \in [-\frac{1}{2}, 0]$.

(ii) There exists a steady state $\bar{v}$, $\bar{\sigma}$ such that for each $x \in [-\frac{1}{2}, 0]$, $v(x, t) \to \bar{v}(x)$, $v_x(x, t) \to \bar{v}_x(x)$, and $\sigma(x, t) \to \bar{\sigma}(x)$ as $t \to \infty$. We emphasize that the steady velocity gradient $\bar{v}_x$ and stress $\bar{\sigma}$ may be discontinuous (as in Fig. 2).

(iii) Let $\bar{v}$, $\bar{\sigma}$ be a steady state such that

$$T'_{\text{steady}}(\bar{v}_x) = g'(\bar{v}_x) + \varepsilon \geqslant \text{const.} > 0. \tag{3.4}$$

(Referring to Fig. 2, inequality (3.4) precludes top and bottom jumping and excludes the region where $T_{\text{steady}}(\bar{v}_x)$ decreases.) Consider a union $\mathcal{U}$ of small subintervals of $-\frac{1}{2} < x < 0$ that are centered at points where $\bar{v}_x$ and $\bar{\sigma}$ are discontinuous. Let smooth initial data be chosen such that $|S(x, 0)|$ is sufficiently small except in $\mathcal{U}$. Then the solution of (M) converges to the steady state $\bar{v}$, $\bar{\sigma}$ on the complement of $\mathcal{U}$. Moreover, the measure of $\mathcal{U}$ can be made arbitrarily small by choosing $|S(x, 0)|$ small enough. In this sense, steady states are stable (even if $\bar{v}_x$ and $\bar{\sigma}$ are discontinuous).

The numerical results discussed in Section 5 suggest that similar results hold for the system (JS). Proofs for (JS) are under investigation.

The model problem (M) was studied also by Hunter and Slemrod [4]. In their construction of the model, the steady-state relation $\bar{\sigma} = g(\bar{v}_x)$ between the stress and strain rate is chosen to be $g_{\mathscr{H}\mathscr{S}}(v_x) := \sigma_{\mathscr{H}\mathscr{S}}(v_x) - \varepsilon v_x$, where the graph of the function $\sigma_{\mathscr{H}\mathscr{S}}$ resembles Fig. 2. In contrast with $\sigma_{\mathscr{J}\mathscr{S}} := T_{\text{steady}}$, $\sigma_{\mathscr{H}\mathscr{S}}$ is independent of ε. Hunter and Slemrod base their analysis on the conservation laws,

$$w_t - u_x = 0, \tag{3.5a}$$

$$\alpha u_t - \alpha_{\mathscr{H}\mathscr{S}}(w)_x = \varepsilon u_{xx} - \alpha u \tag{3.5b}$$

for the acceleration $u = v_t$ and the strain rate $w = v_x$. Therefore jumps in the strain rate v_x are seen to correspond to steady shock waves for the system (3.5) with $\varepsilon = 0$. Based on a local dynamical analysis of shock structure for small ε, the centerline velocity is shown to exhibit hysteresis under quasi-static cycling of the pressure gradient. (This same behavior is observed in the numerical simulation of the system (JS); see Section 5.) We emphasize, however, that this analysis cannot be applied to the model problem (M) as derived from the Johnson–Segalman system (JS) because the function $g_{\mathscr{J}\mathscr{S}}(v_x) := v_x/(1 + v_x^2)$ decays to zero at high strain rate.

3d. *Phase-Plane Analysis*

Quite detailed information about the structure of solutions of (JS) can be garnered by studying a system of ordinary differential equations that approximates it. Motivation for this approximation comes from the following observation: in experiments of Vinogradov, *et al.* [20], $\alpha = \rho h^2 \lambda^2/\mu$ is of the order 10^{-12}; thus the term αv_t in the momentum equation of (JS) is negligible even when v_t is moderately large. We are led to study the approximation to (JS) obtained when $\alpha = 0$. As we now outline, the behavior of solutions of the resulting dynamical system offers an explanation for several features of the flows calculated for the full system (Section 5); in fact, these calculations prompted the following analysis. A detailed exposition of these results is to be found in Ref. [11].

When $\alpha = 0$, the momentum equation may be integrated, just as in the case of steady flows, to show that the total shear stress $T := \sigma + \varepsilon v_x$ coincides with the steady value $\bar{T}(x) = -\hat{f}x$. The remaining equations of (JS) become, for each fixed x, the autonomous planar system of ordinary differential equations

$$\sigma_t = (Z+1)\left(\frac{\bar{T}-\sigma}{\varepsilon}\right) - \sigma, \tag{3.6a}$$

$$Z_t = -\sigma\left(\frac{\bar{T}-\sigma}{\varepsilon}\right) - Z. \tag{3.6b}$$

We emphasize that a different dynamical system is obtained at each point in the channel. These dynamical systems can be analyzed completely by a phase-plane analysis [11], with the following results:

(i) A critical point for the system (3.6) defines a steady-state solution of (JS); such a solution corresponds to a point on the steady total-stress curve (see Fig. 2) at which the total stress is $\bar{T}(x)$. Consequently, there is a single critical point when $\bar{T}$ is sufficiently small or sufficiently large, while there are three critical points when $\bar{T}$ is intermediate in value. A critical point, such as A, that lies between the origin O and the local maximum M of the total-stress curve is an attracting node, which we call a classical attractor. A point, such as C, that lies past the local minimum m is either an an attracting node or an attracting focus, called a spurt attractor. A critical point B lying between M and m is a saddle point. The phase plane for an example with three critical points is shown in Fig. 4, where the invariant manifolds for the classical attractor A and the saddle point B have been drawn. By constructing an invariant region for system (3.6) and analyzing its critical points at infinity, the qualitative structure of orbits for the dynamical system can be determined completely.

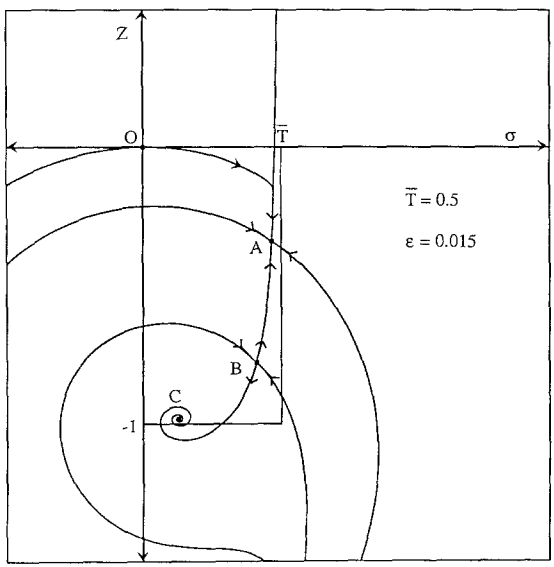

FIG. 4. Phase plane when $\bar{T}$ is subcritical. The critical points A, B, and C are, respectively, an attracting node, a saddle point, and a stable focus.

(ii) Suppose that the initial conditions for the flow are at the origin, $\sigma = 0$ and $Z = 0$, and suppose that the forcing $\bar{f}$ is supercritical. For points x near the centerline, where $\bar{T}(x)$ lies below $\bar{T}_{\text{crit}}$, the origin lies in the basin of attraction of the classical attractor. This is illustrated in Fig. 4, where the integral curve starting at the origin O ends at A. When $\bar{T}(x)$ exceeds $\bar{T}_{\text{crit}}$, the only critical point is the spurt attractor. The orbit through the origin O in this case is shown in Fig. 5. Consequently the flow is predicted to approach a steady spurt solution in which the jump in strain rate occurs at the maximum stress ("top jumping"), with the kink in the velocity profile located as close as possible to the wall. Similar arguments explain the hysteresis effects that occur upon unloading.

(iii) More quantitative information is obtained when ε is small. Referring to Fig. 2, the total stress $\bar{T}_{\text{crit}}$ at the local maximum M is $\frac{1}{2} + O(\varepsilon)$, while the local minimum m corresponds to a total stress of $2\sqrt{\varepsilon}\,[1 + O(\varepsilon)]$. Furthermore, $\sigma = \bar{T} + O(\varepsilon)$ at a classical critical point, while $\sigma = O(\varepsilon)$ for a spurt attractor. Consider a point along the channel for which $\bar{T}(x) > \bar{T}_{\text{crit}}$, so that the only critical point is the spurt attractor, and suppose that $\bar{T} < 1$. Then the evolution of the system exhibits three distinct phases, as indicated in Fig. 5: an initial "Newtonian" phase (O to N); an intermediate "latency" phase (N to S); and a final "spurt" phase (S to C).

The Newtonian phase occurs on a time scale of order ε, during which the system

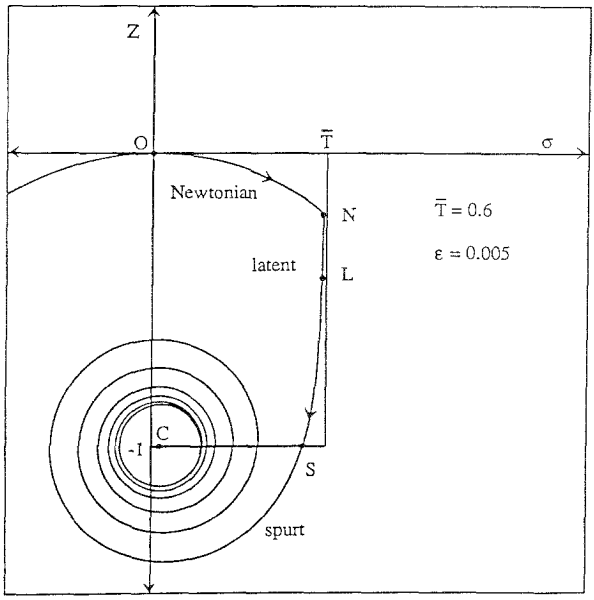

FIG. 5. Phase plane when $\bar{T}$ is supercritical. The point C is the spurt attractor; point L is located at $Z = -1 + \bar{T}$.

approximately follows an arc of a circle centered at $\sigma = 0$ and $Z = -1$. Having assumed that $\bar{T} < 1$, Z approaches

$$Z_{\text{Newton}} = (1 - \bar{T}^2)^{1/2} - 1 \tag{3.7}$$

as σ rises to the value $\bar{T}$. (If, on the other hand, $\bar{T} \geqslant 1$, the circular arc does not extend as far as $\bar{T}$, and σ never attains the value $\bar{T}$; rather, the system slowly spirals toward the spurt attractor. Thus the dynamical behavior does not exhibit distinct phases.)

The latency phase is characterized by having $\sigma = \bar{T} + O(\varepsilon)$, so that σ is nearly constant and Z evolves approximately according to the differential equation

$$Z_t = -\frac{\bar{T}^2}{Z+1} - Z. \tag{3.8}$$

Therefore the shear stress and velocity profiles closely resemble those for a steady solution with no spurt, but the solution is not truly steady because the normal stress difference Z still changes. Integrating Eq. (3.8) from $Z = Z_{\text{Newton}}$ to $Z = -1$ determines the latency period. This period becomes indefinitely long when the forcing decreases to its critical value; thus the persistence of the near-steady solution with no spurt can be very dramatic (see Section 5). The solution remains longest near point L where $Z = -1 + \bar{T}$. This point may be regarded as the remnant of the classical attractor A and the saddle point B.

Eventually the solution enters the spurt phase and tends to the spurt attractor. Because this critical point is a focus, the stress oscillates between the shear and normal components while it approaches the steady state.

4. Numerical Methods

To study the dynamics of system (JS), we developed several different numerical methods; each has its advantages for certain ranges of physical parameters. Calculations with these methods produce similar qualitative and quantitative results.

4a. *Solid Mechanics Formulation*

In the solid mechanics formulation, the system (JS) is regarded as governing the extensional motion of an elastic-plastic bar. The first equation is momentum balance, in which the parabolic term adds viscous "stiffness damping." The remaining equations are incremental constitutive relations for the stress. The stiffness of the material is reflected in the wave speed $[(Z+1)/\alpha]^{1/2}$. We have observed that the wave speed is diminished under loading, so that the material exhibits plastic softening. (See also Ref. [18] for an interpretation of (JS) as governing a viscoplastic material.)

We have solved the system (JS) numerically using a method motivated by solid

mechanics. This method is based on a Galerkin weak form of the momentum equation, with test functions $\phi \in \Phi$ and trial functions $v(\cdot, t) \in \Phi$ for each t. We use continuous piecewise linear functions for Φ, and we represent σ and Z as piecewise constant. The semidiscrete Galerkin equation (integrated by parts) is evaluated at $t_{n+1} = (n+1)\,\Delta t$, yielding

$$\int_{-1/2}^{0} \{\alpha\phi(v_t)_{n+1} + \phi_x \sigma_{n+1} + \varepsilon\phi_x(v_x)_{n+1} - \phi f_{n+1}\}\, dx = 0, \tag{4.1}$$

where $(v_t)_{n+1}$ means $v_t(x, t_{n+1})$, etc. The Galerkin equation is solved for v_{n+1} by advancing the viscoelastic contribution to the stress using a semi-implicit treatment of the constitutive equation:

$$\sigma_{n+1} = (1 - \Delta t)\,\sigma_n + \Delta t Z_n (v_x)_n + \Delta t (v_x)_{n+1}. \tag{4.2}$$

The time derivative is discretized with a trapezoidal approximation, so that

$$v_{n+1} = v_n + \Delta t\{(1-\gamma)(v_t)_n + \gamma(v_t)_{n+1}\} \tag{4.3}$$

for some parameter $\gamma > 0$. The combination of Eqs. (4.1)–(4.3) is a method in which the damping term, which has effective viscosity $\varepsilon + \Delta t$, is treated implicitly, while the nonlinear term involving Zv_x is treated explicitly. The matrix formulation is described in Ref. [9]; as with linear problems, the system matrix needs refactorization only if Δt is changed. After solution of the combined equations for v_{n+1}, σ is corrected and Z is advanced according to

$$\begin{aligned} \sigma_{n+1} &= (1 - \Delta t)\,\sigma_n + \Delta t(Z_n + 1)(v_x)_{n+1} \\ Z_{n+1} &= (1 - \Delta t)\, Z_n - \Delta t \sigma_{n+1}(v_x)_{n+1}. \end{aligned} \tag{4.4}$$

Other variants of (4.4) that treat the constitutive equations with a higher degree of implicitness are obvious. However, as long as they are combined with (4.2), which limits the scheme to first-order accuracy in time, there is no reason to expect such variants to be more accurate. They may improve stability, but the algorithm, as given, is very stable.

The stability of this method has been analyzed for the system (JS) with Z frozen [12]: the method is stable provided that $Z + 1 > -\varepsilon$ and the time step is restricted by $\Delta t < 2$ (i.e., $\Delta t < 2/\lambda$, dimensionally). Of course, if $Z + 1 \leqslant -\varepsilon$, then the differential equations themselves, as well as the method, are linearly unstable.

4b. *Parabolic Formulation*

Recall that the total stress is defined to be $T = \sigma + \varepsilon v_x$; assume that $\varepsilon > 0$. Introducing T as an independent variable, the system (JS) is replaced by

$$T_t = \frac{\varepsilon}{\alpha} T_{xx} + (Z+1)\left(\frac{T-\sigma}{\varepsilon}\right) - \sigma, \tag{4.5a}$$

$$\sigma_t = (Z+1)\left(\frac{T-\sigma}{\varepsilon}\right) - \sigma, \tag{4.5b}$$

$$Z_t = -\sigma\left(\frac{T-\sigma}{\varepsilon}\right) - Z. \tag{4.5c}$$

The boundary conditions are $T_x(-\frac{1}{2}, t) = -f$ and $T(0, t) = 0$. The velocity profile may be reconstructed by integrating $(T-\sigma)/\varepsilon$.

The system (4.5) has the form of a linear heat equation forced by a nonlinear heat source that is governed by two auxiliary ordinary differential equations. To solve this system numerically, we discretize the parabolic term in Eq. (4.5a) implicitly while treating the remaining forcing terms explicitly. Time integration is performed using a packaged ordinary differential equation solver.

We remark that system (4.5) is convenient also for studying existence and regularity of solutions of (JS).

4c. *Conservative Formulation*

The system (JS) is equivalent to the system (C); therefore it may be studied from the viewpoint of conservation laws. In Ref. [18], we have determined completely the structure of scale-invariant nonlinear waves for (C) when $\varepsilon = 0$. Such a wave consists of a sequence of elementary scale-invariant waves, either centered discon-

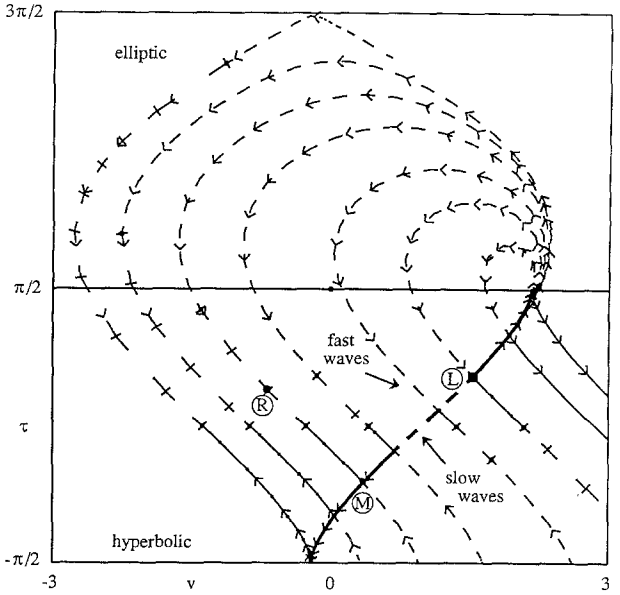

FIG. 6. The wave curve diagram (schematic) for a typical U_L. Solid curves correspond to rarefaction waves, dashed curves to shock waves, and dashed curves with crossbars to composite waves. Darker curves represent the $-c$ family, while lighter curves represent the $+c$ family.

tinuities or rarefaction waves, connecting constant states on the left and right. Discontinuities are required to satisfy Liu's generalization of Oleĭnik's entropy condition, which guarantees that energy is dissipated (cf. Eq. (3.3)). This admissibility condition is equivalent to requiring shock waves to have viscous profiles: admissible shock waves arise as limits of traveling-wave solutions of (C) as $\varepsilon \to 0$. Our analysis follows the techniques for general systems of conservation laws discussed in Refs. [14, 5].

The wave structure is conveniently depicted with a wave curve, the locus of states $U = (\tau, v, z)$ on the right for a fixed state $U_L = (\tau_L, v_L, z_L)$ on the left. Only z may change across waves with zero speed, so these wave curves are trivial. On the other hand, z remains constant across waves corresponding to the characteristic families with speeds $\pm c$, so we suppress the z component of U when drawing wave curves. Figure 6 shows the wave curve of the $-c$ (i.e., slow) family for a representative initial state U_L; through points along this curve are drawn the wave curves of the $+c$ (i.e., fast) family. The figure was produced using a computer program that constructs the wave curves for general systems of conservation laws [5].

With the structure of scale-invariant waves known, Riemann initial-value problems may be solved. This is illustrated in Fig. 6 for the Riemann problem with left state U_L and right state U_R: the solution contains the middle state U_M separating a slow composite wave on the left from a fast composite wave on the right. We have written a computer program that solves Riemann problems and have incorporated it into the Glimm–Chorin random choice method. This method solves the Cauchy problem without introducing artificial Newtonian viscosity. We refer to Ref. [17] for a detailed discussion.

5. Numerical Results

In this section we describe several features of the shear flow of a Johnson–Segalman fluid, as obtained using the numerical methods of Section 4.

5a. *Effects of Newtonian Viscosity*

As our first numerical experiment, we simulated system (C) with $\varepsilon = 0$ using the random choice method. Parameters were chosen so that $\alpha = 1$. The flow was

value $1.2 f_{\text{crit}}$.

The result is shown in Fig. 7. The fluid velocity v is plotted vs position x at successive time intervals; generally the velocity increases with time. During the early stages of the experiment, the flow settled into a quasi-steady state. This latency effect is especially evident in a plot of the centerline velocity as a function of time, and it is more pronounced when α is smaller. Eventually, however, a thin layer develops at the plate in which the velocity rises to a value that is nearly constant across the channel. For practical purposes, the fluid has broken free from the plate

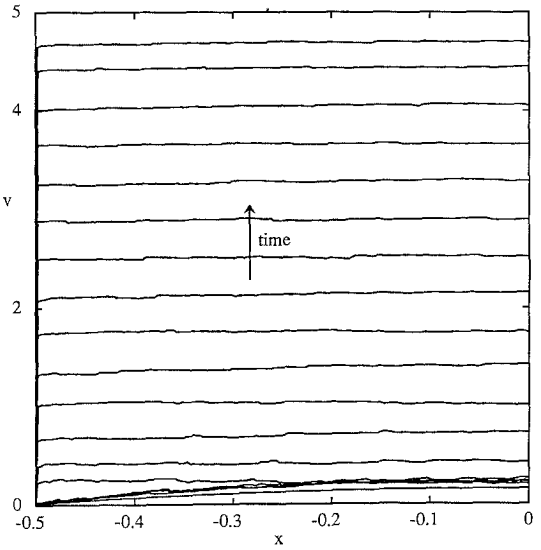

FIG. 7. Onset of slip for a fluid without Newtonian viscosity.

and is accelerating uniformly under the applied pressure gradient; thus the fluid "slips." This occurrence might be related to the phenomenon of wall slip, which has been associated with non-monotone constitutive relations [2, 10].

It is worth noting that the random choice method is the only numerical method that can calculate super-critical flows with $\varepsilon = 0$: other methods must be stabilized with artificial viscosity when the flow is discontinuous. This is important because some fluids that exhibit spurt have negligible Newtonian viscosity. (For these fluids, the relation between steady stress and strain rate resembles Fig. 2 because of multiple relaxation time scales [11].)

The same experiment was performed for system (C) with a small, but nonzero, Newtonian viscosity coefficient ε. Figure 8 shows the results for $\varepsilon = 0.01$, as calculated using the Lax–Wendroff method with Tyler artificial viscosity. What results is a different phenomenon, in which the shorter relaxation response of the fluid (here modeled by Newtonian viscosity) arrests the acceleration in a layer near the wall. Now the slip layer is much thicker, with its outer boundary corresponding to a discontinuity in the strain rate v_x. The solution approaches a steady state in which v_x is discontinuous but the total stress $T = \sigma(v_x) + \varepsilon v_x$ is continuous. The steady state has the same layer thickness as predicted analytically, but the centerline velocity is 20% too high; this is because the centerline velocity is extremely sensitive to the slope of the velocity profile in the slip layer, which is affected by the artificial viscosity in the numerical method. The layer formation is crucial to our interpretation of the spurt phenomenon.

More extensive experiments were performed using the solid mechanics algorithm. For example, the calculation of Fig. 8 was repeated using this method and a graded

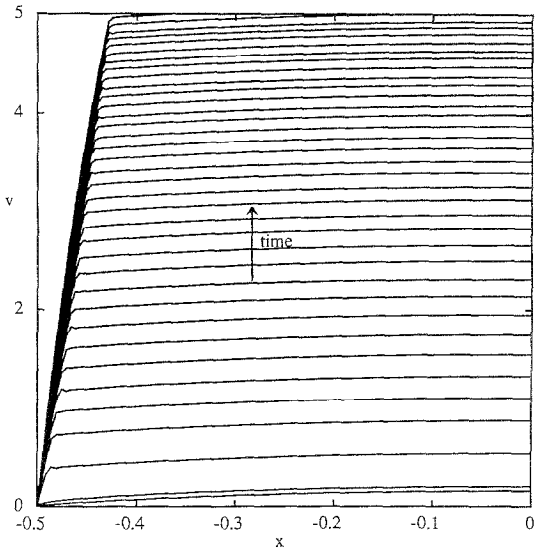

FIG. 8. Onset of spurt for a fluid with Newtonian viscosity.

mesh of 160 elements; the same layer thickness as shown in Fig. 8 was obtained, and the centerline velocity of the long-time solution differed from the analytic prediction by about only 1%.

5b. *Spurt Phenomenon*

We used the solid mechanics approach to simulate the experiments of Vinogradov, *et al.* with polyisoprene [20]. In these experiments, the sample fluids are labeled PI-1 through PI-8, ordered by increasing molecular weight M; the parameters entering the mathematical model were chosen to correspond to these samples. In the system (JS), α measures the relative importance of inertial and elastic effects, and ε reflects the presence of Newtonian viscosity. For the experimental fluids, however, the Newtonian viscosity is negligible because there is no solvent; instead the fluids exhibit a second relaxation time that is much shorter than the dominant relaxation time λ^{-1}. Nevertheless, the effects of a short secondary relaxation time are correctly modeled by the Newtonian viscosity term provided that ε is interpreted as the ratio of the relaxation times [11].

The following features of the experimental fluids samples were used to determine the physical constants:

(i) The elastic modulus μ is independent of the molecular weight M.

(ii) The contribution to the zero shear viscosity from the dominant relaxation time, μ/λ, varies over two orders of magnitude because of the sensitive dependence of λ^{-1} on M.

(iii) There is a critical molecular weight below which the material does not spurt. (Samples PI-1 and PI-2 do not exhibit spurt.)

(iv) For samples PI-3, PI-8, the critical stress for onset of spurt is independent of M.

These observations, together with the presumption that the secondary relaxation time is independent of M, lead to values for α and ε that decrease with M and a value of $a = 0.98$. These values are obtained readily from our definitions in Section 2 and the dimensional information given in Ref. [9]; they are given for each of the Vinogradov fluids in Table I. The computational results are shown in Figs. 9–11.

Figure 9 shows the evolution of the spurt process in time; the centerline velocity is plotted vs. time for sample PI-7 with $\bar{f} = 1.2$. The spatial mesh, with a total of 640 elements, was graded to have smaller elements near the wall. All simulations were carried out using zero initial data. Not visible in Fig. 9 is a "start-up" transient, occurring on a time scale of order ε, during which the centerline velocity spikes to a large value corresponding to a Newtonian fluid with viscosity ε. Following this is a "latency" period when the velocity and the shear stress resemble a steady solution without spurt. This period ends at $t = 2.36$ (i.e., 376 s, dimensionally), when a spurt solution begins to develop. Notice that these three phases of the dynamics correspond to the results of the phase-plane analysis of Section 3c. Moreover, the latency time observed in the full dynamical simulations correlates precisely with the value $t = 2.36$ found by integrating the ordinary differential equations; it also agrees with the predictions of Eq. (3.8), which gives $t = 2.30$ (see Ref. [11]).

The calculation shown in Fig. 9 has not been run long enough to achieve steady state. Essentially steady flow is attained after about five more time units; thus we predict that the whole dynamic process for this experimental sample takes about 40 min. We have run complete simulations for each of the eight samples. Figure 10 shows the results, as compared to the data reported in Ref. [20]. In these graphs, effective shear rate S is plotted vs. effective wall shear stress $\bar{T}_{\text{wall}} = \bar{f}h/2$; here the effective shear rate is $S = 4Q/\pi R^3$ for a capillary of radius R and $S = 6Q/(wh^2)$ for a slit die of width w, Q being the volumetric flow rate [9].

Figure 11 shows the result of simulating a loading sequence in which the pressure gradient $\bar{f}$ is increased in small steps, allowing sufficient time between steps to achieve steady flow [9]. The loading sequence is followed by a similar unloading

TABLE I

Nondimensional Groups α and ε Corresponding to the Data of Vinogradov *et al.* [20], Fit by the Power Laws of Ref. [9]

	PI-1	PI-2	PI-3	PI-4	PI-5	PI-6	PI-7	PI-8
$\alpha \times 10^{10}$	400	44.2	0.627	0.137	0.0876	0.0438	0.00569	0.00420
ε	0.376	0.125	0.0149	0.00697	0.00557	0.00394	0.00142	0.00122

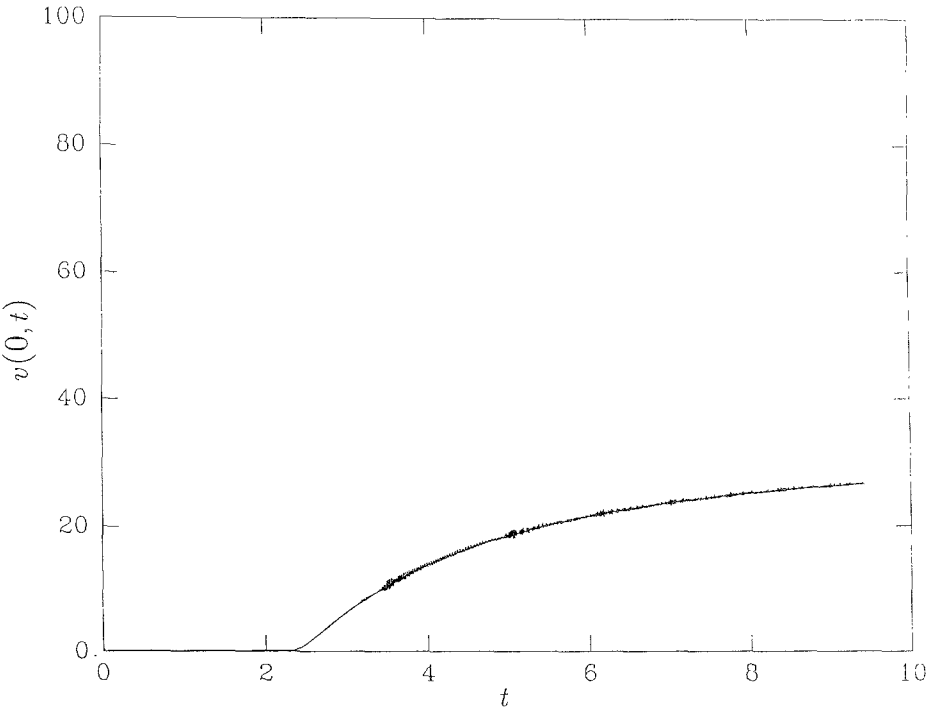

FIG. 9. Centerline velocity vs. time.

sequence, in which the driving gradient is decreased in steps. The initial step used zero initial data, and succeeding steps used the results of the previous step as initial data. The resulting hysteresis loop resembles the "shape memory" observed by Hunter and Slemrod [4] in their model system (3.5). The width of the hysteresis loop at the bottom can be related directly to the molecular weight of the sample [9] (see Section 6).

5c. *Performance of the Numerical Methods*

Of the numerical methods we have proposed, the random choice method is the only one that applies to the interesting case in which $\varepsilon = 0$; the physical ramifica-

explicit, this method is restricted to values of α that are not too small. (Recalling that the wave speed is $\sqrt{(Z+1)/\alpha}$, the number of time steps required to reach time t is $O(Nt/\sqrt{\alpha})$ for a calculation with N spatial mesh cells.) When $\varepsilon \neq 0$, the solid mechanics approach yields the most fully developed and flexible method. The parabolic method may have advantages, but we have not attempted to refine it; our implementation is as simple as possible, relying heavily on packaged codes, so as to confirm the validity of the other two methods.

Computations in the experimental regime yield interesting insights into the

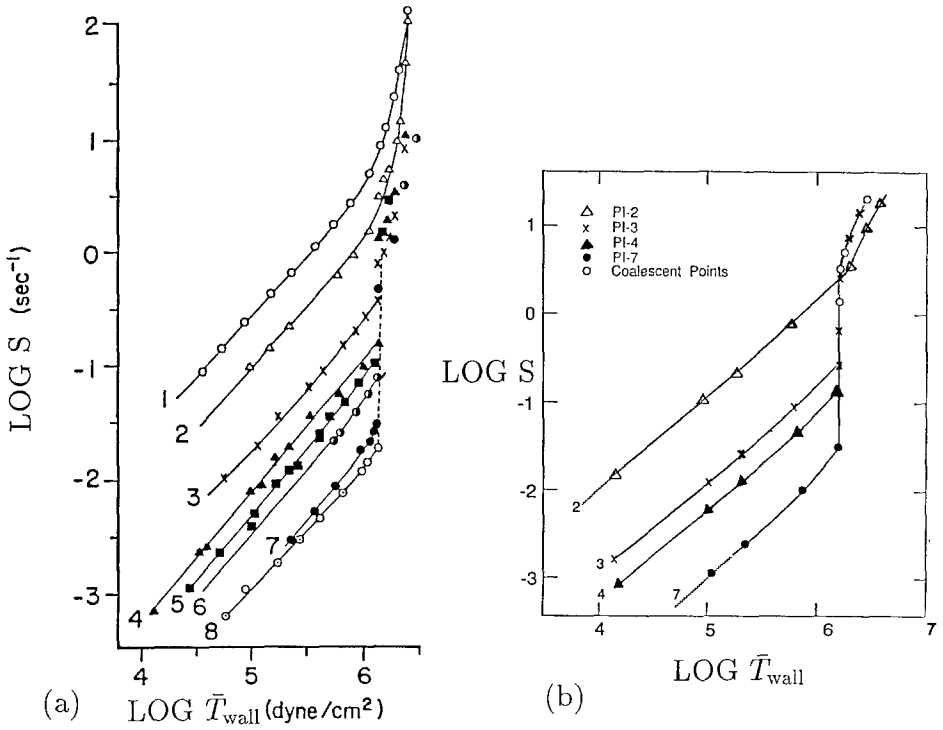

FIG. 10. Volumetric flow rate vs. effective shear stress: (a) experiment [20]; (b) numerical calculation [9]. Notice that the horizontal scale of this panel matches that of panel (a), but the vertical scale does not.

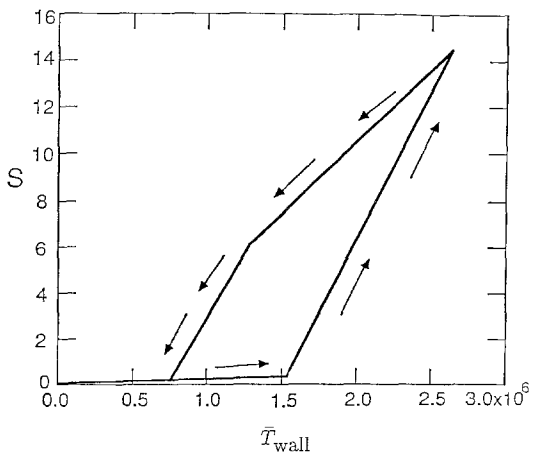

FIG. 11. Hysteresis under cyclic loading.

behavior of our numerical methods; a case in point is the phenomenon of latency. To accurately reproduce the latency time predicted by phase-plane analysis, Δt must be relatively small compared to ε during the transient "Newtonian" phase, which takes place on a time-scale of order ε. Figure 9 was generated using 100 time steps with $\Delta t = \varepsilon/10$, followed by 7500 steps with $\Delta t = \varepsilon/1.13$. When the time step is larger, the solid mechanics algorithm remains stable, but accuracy is sacrified; thus the normal stress difference Z at the end of the Newtonian phase is not calculated precisely. Indeed, if equal time steps are used throughout the simulation, the latency time is computed to be $t = 2.14$. That this value compares favorably with $t = 2.36$ reflects the robustness of the algorithm. By constrast, there is no semi-implicit treatment in our version of the parabolic method, which requires a time step smaller than does than the solid mechanics approach.

We have been careful to test the validity of the numerical results we report here. One of the questions we sought to resolve involves the oscillations evident in Fig. 9 during the spurt process. In Ref. [9], results were reported on meshes much cruder than the one used to compute the results of Fig. 9; the oscillations were larger in amplitude, and they did not diminish with refinement of time step. Figure 9 shows that these oscillations diminish with refinement of the spatial grid size, suggesting that they are induced by spatial discretization error. This conclusion is reinforced by inspection of Fig. 9: the larger oscillations occur somewhat after the onset of spurt, when the layer boundary has moved out of the region of mesh refinement near the wall. Eventually, however, these oscillations are damped, just as they are in calculations with cruder meshes. Further mesh refinement studies indicate that although crude spatial resolution can lead to spurious oscillations in spurt dynamics, the solution maintains an accurate mean value and approaches the correct steady state. These results were reproduced using the parabolic formulation with a mesh refined to 3072 equal-sized cells. To obtain accurate estimates of latency time with this method, the time step must be about half of that required by the solid mechanics method; if this condition is violated, the spurt occurs prematurely (but the steady states achieved are accurate). When the time step is so refined, the results obtained with both methods agree to graphical accuracy.

Our numerical approaches have successfully computed fully time-dependent flows for a Johnson–Segalman fluid at a high Deborah number. Thus they avoid the "high Weisenberg/Deborah number problem," at least in one-dimensional flows. Currently, we are investigating generalizations of our approaches to multi-dimensional problems of physical interest.

6. Rheological Experiments

In Ref. [9], several possible experiments are suggested that could verify the interpretation of spurt put forward here. The most important experiment suggested is the verification of the molecular-weight dependence of the widest point of the hysteresis loop of Fig. 11.

The shape of the hysteresis loop is a key feature predicted by our analysis and computations: the loop always opens from the point at which unloading begins, and there is a discontinuity in slope during unloading. This is because the solutions proceed from "top-jumping" in Fig. 2, through intermediate convexifications of the curve, to "botton-jumping," causing the discontinuity in slope. (This behavior is in distinct contrast to the interpretation of Ref. [13], where bottom-jumping is always the rule for steady spurt solutions, and portions of the loading path are retraced during unloading.) The critical wall stress for onset of spurt under loading is $\bar{T}_{\text{crit}} = \frac{1}{2} + O(\varepsilon)$, whereas spurt does not cease when unloading until the wall stress drops below $2\sqrt{\varepsilon}[1 + O(\varepsilon)]$. The sensitive dependence of ε on the molecular weight leads to observable variation in the hysteresis loop.

The analysis and computations presented in this paper allow us to say more about experimental signatures: (i) before dramatic growth in throughput occurs, very slow flow with little throughput persists during a latency period that can last several minutes; (ii) latency occurs only when ε is sufficiently small (i.e., less than 1/8 for Johnson–Segalman; the precise number for other models may be different); (iii) latency occurs only if the applied pressure gradient is not too large ($\bar{f}_{\text{crit}} < \bar{f} < 2$ for Johnson–Segalman); (iv) the latency time scales with λ^{-1} when the pressure gradient is fixed, and is determined approximately by integrating Eq. (3.8).

7. Conclusion

Well-posed dynamical problems for fluids with non-montone constitutive relations need not be unphysical. In fact, the Johnson–Segalman model provides a relatively simple example that accurately describes spurt. Our analytical and computational results predict several phenomena related to spurt, which should be observable in rheological experiments.

Acknowledgments

We thank R. W. Kolkka, W. G. Pritchard, and A. E. Tzavaras for many helpful discussions. We are also grateful to M. Yao for his help with the figures.

References

1. R. Bird, R. Armstrong, and O. Hassager, *Dynamics of Polymeric Liquids* (Wiley, New York, 1987).
2. M. Doi and S. Edwards, *J. Chem. Soc. Faraday* **74**, 1789 (1978).
3. C. Guillopé and J.-C. Saut, Global existence and one-dimensional nonlinear stability of shearing motions of viscoelastic fluids of Oldroyd type, 1989; *Math. Modell. Num. Anal.*, in press.
4. J. Hunter and M. Slemrod, *Phys. Fluids* **26**, 2345 (1983).
5. E. Isaacson, D. Marchesin, and B. Plohr, Construction of nonlinear waves for conservation laws, in preparation.

6. D. JOSEPH, M. RENARDY, AND J.-C. SAUT, *Arch. Rat. Mech. Anal.* **87**, 213 (1985).
7. D. JOSEPH AND J.-C. SAUT, *J. Non-Newtonian Fluid Mech.* **20**, 117 (1986).
8. M. JOHNSON AND D. SEGALMAN, *J. Non-Newtonian Fluid Mech.* **2**, 255 (1977).
9. R. KOLKKA, D. MALKUS, M. HANSEN, G. IERLEY, AND R. WORTHING, *J. Non-Newtonian Fluid Mech.* **29**, 303 (1988).
10. Y.-H. LIN, *J. Rheol.* **29**, 609 (1985).
11. D. MALKUS, J. NOHEL, AND B. PLOHR, Analysis of new phenomena in shear flows of non-Newtonian fluids, submitted.
12. D. MALKUS. Y.-C. TSAI, AND R. KOLKKA, New transient algorithms for non-Newtonian flows, in *Finite Elements in Fluids, Vol. 8*, edited by T. Chung (Hemisphere Publishing Corp., New York, to appear).
13. T. MCLEISH AND R. BALL, *J. Polymer Sci.* **24**, 1735 (1986).
14. R. MENIKOFF AND B. PLOHR, *Rev. Mod. Phys.* **61**, 75 (1989).
15. J. NOHEL, R. PEGO, AND A. TZAVARAS, Stability of discontinuous steady states in shearing motions of a non-Newtonian fluid, *Proc. Royal Soc. Edinburgh, Series A*, accepted.
16. J. PEARSON, *Mechanics of Polymer Processing* (Elsevier Appl. Sci., London, 1985).
17. B. PLOHR, *AIAA J.* **26**, 470 (1988).
18. B. PLOHR, in *Workshop on Partial Differential Equations and Continuum Models of Phase Transitions, Nice, 1988*, edited by D. Serre (Springer-Verlag, New York, 1989).
19. M. RENARDY, W. HRUSA, AND J. NOHEL, *Mathematical Problems in Viscoelasticity* (Longman Sci. & Tech. Essex, England, 1987).
20. G. VINOGRADOV, A. MALKIN, YU. YANOVSKII, E. BORISENKOVA, B. YARLYKOV, AND G. BEREZHNAYA, *J. Polym. Sci. Part A-2* **10**, 1061 (1972).